

# SAR tomography for the retrieval of forest biomass and height: cross-validation at two tropical forest sites in French Guiana

Dinh Ho Tong Minh<sup>a,b</sup>, Thuy Le Toan<sup>b</sup>, Fabio Rocca<sup>c</sup>, Stefano Tebaldini<sup>c</sup>, Ludovic Villard<sup>b</sup>, Maxime Réjou-Méchain<sup>d,e</sup>, Oliver L Phillips<sup>f</sup>, Ted R. Feldpausch<sup>g</sup>, Pascale Dubois-Fernandez<sup>h</sup>, Klaus Scipal<sup>i</sup>, Jérôme Chave<sup>d</sup>

<sup>a</sup>*Institut national de Recherche en Sciences et Technologies pour l'Environnement et l'Agriculture (IRSTEA), UMR TETIS, Montpellier, France*

<sup>b</sup>*Centre d'Etudes Spatiales de la Biosphère (CESBIO), UMR CNRS 5126, University of Paul Sabatier, Toulouse, France*

<sup>c</sup>*Dipartimento di Elettronica, Informazione e Bioingegneria, Politecnico di Milano, Milano, Italy*

<sup>d</sup>*Laboratoire Evolution et Diversite Biologique, UMR CNRS 5174, University of Paul Sabatier, Toulouse, France*

<sup>e</sup>*French Institute of Pondicherry, UMIFRE 21/USR 3330 CNRS-MAEE, Pondicherry, India*

<sup>f</sup>*School of Geography, University of Leeds, University Road, Leeds LS2 9JT, UK*

<sup>g</sup>*Geography, College of Life and Environmental Sciences, University of Exeter, UK*

<sup>h</sup>*Office National d'Etudes et de Recherches Aérospatiales (ONERA), Toulouse, France*

<sup>i</sup>*European Space Research and Technology Centre (ESTEC), Noordwijk, the Netherlands*

---

## Abstract

Developing and improving methods to monitor forest carbon in space and time is a timely challenge, especially for tropical forests. The next European Space Agency Earth Explorer Core Mission BIOMASS will collect synthetic aperture radar (SAR) data globally from employing a multiple baseline orbit during the initial phase of its lifetime. These data will be used for tomographic SAR (TomoSAR) processing, with a vertical resolution of about 20 m, a resolution sufficient to decompose the backscatter signal into two to three layers for most closed-canopy tropical forests. A recent study, con-

ducted in the Paracou site, French Guiana, has already shown that TomoSAR significantly improves the retrieval of forest aboveground biomass (AGB) in a high biomass forest, with an error of only 10% at 1.5-ha resolution. However, the degree to which this TomoSAR approach can be transferred from one site to another has not been assessed. We test this approach at the Nouragues site in central French Guiana (ca 100 km away from Paracou), and develop a method to retrieve the top-of-canopy height from TomoSAR. We found a high correlation between the backscatter signal and AGB in the upper canopy layer (i.e. 20-40 m), while lower layers only showed poor correlations. The relationship between AGB and TomoSAR data was found to be highly similar for forests at Nouragues and Paracou. Cross validation using training plots from Nouragues and validation plots from Paracou, and vice versa, gave an error of 16 - 18% of AGB using 1-ha plots. Finally, using a high-resolution LiDAR canopy model as a reference, we showed that TomoSAR has the potential to retrieve the top-of-canopy height with an error to within 2.5 m. Our analyses show that the TomoSAR-AGB retrieval method is accurate even in hilly and high-biomass forest areas and suggest that our approach may be generalizable to other study sites, having a canopy taller than 30 m. These results have strong implications for the tomographic phase of the BIOMASS spaceborne mission.

*Keywords:* Aboveground biomass, BIOMASS mission, French Guiana, Paracou, Nouragues, TropiSAR, P-band SAR tomography, tomography phase, vertical forest structure

---

## 1. Introduction

Forests play a key role in the global carbon cycle, and hence in the global climate (Wright, 2005; Pan et al., 2011). However, this role remains poorly characterized quantitatively, as compared to other ecosystems due to the practical difficulties in measuring forest biomass stocks over broad scales. Over the past few years, considerable progress has been made in mapping forest ecosystem biomass stocks using a range of remote sensing technologies (Saatchi et al., 2011b; Baccini et al., 2012; Mitchard et al., 2009; Mermoz et al., 2015). However, these studies have limitations associated with limited sensor sensitivity to biomass, inappropriate sampling intensity, and limited validation of the methodology. These maps are least accurate in high carbon stock forests, predominantly found in the tropics, where existing large-scale remotely-sensed biomass maps conflict substantially with field-based estimates of spatial biomass patterns (e.g., (Mitchard et al., 2014)). Tropical forests are highly complex, varied, and often threatened. In this context there is a critical need to develop new technologies that can help survey and monitor tropical forests.

Delivering accurate global maps of forest aboveground biomass (AGB) and height is the primary objective of BIOMASS, the next European Space Agency (ESA) Earth Explorer Core Mission (Le Toan et al., 2011). The BIOMASS satellite is planned for a 2020 launch date. To achieve the goal of wall-to-wall mapping of forest AGB, the BIOMASS mission features, for the first time from space, a fully polarimetric, P-band (435 MHz,  $\sim 69$  cm wavelength, and 6 MHz bandwidth) Synthetic Aperture Radar (SAR). The low frequency ensures that the transmitted wave can penetrate the vegeta-

26 tion down to the ground even in dense multi-layer tropical forests (Smith-  
27 Jonforsen et al., 2005; Ho Tong Minh et al., 2014a). The satellite will operate  
28 in two different observation phases. The tomographic phase will last for one  
29 year and will result in one global forest AGB and total canopy height map at  
30 200-m resolution. It will be followed by an interferometric phase, which will  
31 last for four years and will provide updated global forest AGB maps every  
32 six months (Ho Tong Minh et al., 2015b).

33 The algorithm for forest AGB retrieval based on P-band SAR has been  
34 developed during the BIOMASS Mission Assessment Phase (Phase A), based  
35 on airborne data collected over boreal and tropical forests (Sandberg et al.,  
36 2011; Ho Tong Minh et al., 2014a; Villard and Le Toan, 2015). It makes  
37 full use of information on Polarimetric SAR (PolSAR) backscatter intensity  
38 and the Polarimetric Inteferometric (PolInSAR) phase information. PolSAR  
39 algorithms combine statistical and physical models to derive AGB based on  
40 intensity measurements in all polarizations (Le Toan et al., 1992; Sandberg  
41 et al., 2011). These algorithms usually perform better for low biomass values  
42 (typically less than 200 t/ha in dry matter units), whereas at high AGB, sig-  
43 nal intensity exhibits a saturation effect that affects biomass retrieval. PolIn-  
44 SAR technique combines two PolSAR measurements from slightly different  
45 orbits to obtain an estimate of forest height; this canopy height is subse-  
46 quently converted into AGB using field-derived allometric equations (Saatchi  
47 et al., 2011a; Le Toan et al., 2011). By combining AGB estimates from these  
48 two complementary techniques, AGB maps may be produced with less than  
49 20% root mean square error (RMSE), at a resolution of 4-ha (Le Toan et al.,  
50 2011). To achieve this performance, however, AGB estimation algorithms

51 need to be accurately tuned, so as to take into account noise factors that af-  
52 fect radar measurements, primarily terrain topography and ground moisture  
53 status (Ho Tong Minh et al., 2014a; Van Zyl, 1993).

54 The analysis and evaluation of data collected during the tomography  
55 phase is essential to achieving the goals of the BIOMASS mission. The  
56 satellite’s orbit is designed to gather multiple acquisitions over the same  
57 sites from slightly different orbital positions, so as to image forest vertical  
58 structure through SAR tomography (henceforth referred to as TomoSAR)  
59 (Reigber and Moreira, 2000; Ho Tong Minh et al., 2015b). Hence, for the  
60 first time, BIOMASS will provide quantitative information on forest structure  
61 through P-band TomoSAR from space.

62 The potential of P-band TomoSAR to characterize forest structure was  
63 previously assessed in a number of studies relating forest vertical structure to  
64 forest biomass (Tebaldini and Rocca, 2012; Mariotti d’Alessandro, M. et al.,  
65 2013; Ho Tong Minh et al., 2014a). The TropiSAR campaign carried out  
66 in 2009 in French Guiana offered the first opportunity to test TomoSAR  
67 for tropical forest areas (Dubois-Fernandez et al., 2012). TropiSAR data  
68 have been acquired for TomoSAR processing at two forest sites, the Paracou  
69 forest and the Nouragues forest, about 100 km apart. In a previous study  
70 we conducted at the Paracou site, the signal at P-band coming from upper  
71 vegetation layers was found to be strongly correlated with forest AGB, for  
72 values ranging from 250 t/ha to 450 t/ha (Ho Tong Minh et al., 2014a). This  
73 finding was used to construct a simple AGB model having a RMSE of only  
74 10% at a resolution of 1.5 ha. These results suggest that TomoSAR methods  
75 hold promise for accurately mapping forest biomass in tropical areas.

76 The robustness of the TomoSAR algorithm, however, needs further eval-  
77 uation to different sites. Here we provide the first such assessment by per-  
78 forming a cross-comparison between two French Guiana tropical forest sites,  
79 namely Paracou and Nouragues. In addition we report on the performance  
80 of forest top height retrieved from the TomoSAR data at both sites. Specif-  
81 ically, we address the following questions: (1) Can the TomoSAR algorithm  
82 be parameterized for a landscape on hilly terrain?; (2) Is the relationship  
83 between TomoSAR and AGB transferable across tropical forest sites?; (3)  
84 Is the forest top height retrieval algorithm transferrable? Finally we discuss  
85 the implications of these findings for the tomographic phase of the BIOMASS  
86 spaceborne mission.

## 87 **2. Methods**

### 88 *2.1. Field data*

89 The present study was conducted at two sites in French Guiana. The first  
90 site, the Nouragues Ecological Research Station, is located 120 km south of  
91 Cayenne, French Guiana (4°05' N, 52°40' W). This area is a protected natural  
92 reserve characterized by a lowland moist tropical rainforest. The climate is  
93 humid with a mean annual rainfall of 2861 mm/year (average 1992-2012),  
94 a short dry season in March and a longer 2-month dry season from late  
95 August to early November. The site is topographically heterogeneous, with  
96 a succession of hills ranging between 26-280 m above sea level (asl) and a  
97 granitic outcrop (Inselberg) reaching 430 m asl (the mean ground slope is  
98 greater than 5° at a 100-m resolution). The study area encompasses three  
99 main types of geological substrates, a weathered granitic parent material

100 with sandy soils of variable depths, a laterite crust issued from metavolcanic  
101 rock of the Paramaca formation with clayey soils and a metavolcanic parent  
102 material. There has been no obvious forest disturbance by human activities  
103 in the past 200 years. One hectare of forest includes up to 200 tree species  
104 with a diameter at breast height (DBH)  $\geq 10$  cm. Top-of-canopy height  
105 reaches up to 55 m with the average value around 35 m. At Nouragues,  
106 ground-based AGB was inferred from two large and long term permanent  
107 plots, namely Grand Plateau (1000 x 100  $m^2$ ) and Petit Plateau (400 x 300  
108  $m^2$ ), both established in 1992-1994 and regularly surveyed to the present.  
109 The two plots were subdivided in 100 x 100  $m^2$  subplots, resulting in 22  
110 study plots of 1-ha. We used tree census data conducted at the end of 2008.  
111 Five additional plots were also considered in the analyses, three of 1-ha (100  
112 x 100  $m^2$ ) in terra-firme forest (Pararé-ridge established in 2010; Lhor in  
113 2010; Ringler in 2012) and two 0.25-ha plots (50 x 50  $m^2$ ) in permanently  
114 flooded forests (Bas\_fond 1 and Bas\_fond 2 both in 2012).

115 The second study area is located at the Paracou station, near Sinnamary,  
116 French Guiana (5°18' N, 52°55' W). The climate is also humid with a mean  
117 annual rainfall of 2980 mm/year (30 years period) and a 2-month dry season  
118 occurring from late August to early November. The Paracou site is fairly  
119 flat and has a homogeneous topography (5-50 m asl), but with deep drainage  
120 gullies flowing into the Sinnamary River. The most common soils at Para-  
121 cou are shallow ferralitic soils which are limited in depth by a more or less  
122 transformed loamy saprolithe (Gourlet-Fleury et al., 2004). Following forest  
123 censuses, the number of tree species is estimated to be approximately 140-  
124 160 species/ha (trees with DBH  $\geq 10$  cm). Top-of-canopy height reaches

125 up to 45 m with the average value around 30 m. In Paracou, in-situ forest  
126 measurements were available from 16 permanent plots established since 1984.  
127 There are 15 plots of 250 x 250  $m^2$  (6.25 ha) and one plot of 500 x 500  $m^2$   
128 (25 ha). From 1986 to 1988, nine of these 15 6.25-ha plots underwent three  
129 different mild to severe logging treatments to study forest regeneration after  
130 logging (Gourlet-Fleury et al., 2004). Logging treatments had a significant  
131 impact on current AGB stocks (Blanc et al., 2009). As at the Nouragues  
132 site, we subdivided these large plots in 100 x 100  $m^2$ . This resulted in 85  
133 field plot units for the Paracou site. To match the BIOMASS resolution, we  
134 also subdivided all large plots in 200 x 200  $m^2$  subplots, resulting in 19 4-ha  
135 plots.

136 At both sites, the two forests are moist closed-canopy tropical forests.  
137 Nouragues forest has a slightly higher top canopy and aboveground biomass  
138 stock and is on a more hilly terrain. However, the floristic composition is  
139 largely similar (dominant tree families are Fabaceae, Sapotaceae, Burser-  
140 aceae, Lecythidaceae, Chrysobalanaceae, and Moraceae), and is typical of  
141 most forests at the north-eastern end of the long pan-Amazon floristic gra-  
142 dient (e.g., (ter Steege et al., 2006)).

143 In each permanent sampling plot, living trees  $\geq 10$  cm DBH were mapped,  
144 diameter measured to the nearest 0.5 cm at 1.3 m above the ground, and  
145 botanically identified when possible. For trees with buttresses, stilt roots or  
146 irregularities, stem diameter was measured 30 cm above the highest irregu-  
147 larity. The point of measurement was marked with permanent paint on the  
148 stem. Trees  $\leq 10$  cm DBH and lianas were disregarded in the census, but  
149 these contribute a small fraction of the total AGB.



150 A subset of tree heights was measured at Nouragues (2462 trees) and  
151 Paracou (1157 trees). These were used to construct plot-specific height-  
152 diameter allometries in each plot using a model of the form:

$$\ln(H) = a + b \times \ln(DBH) + c \times \ln(DBH)^2 \quad (1)$$

153 where  $H$  is the total tree height (Rejou-Mechain et al., 2015). In Paracou,  
154 a single height diameter model was used for all 6.25-ha plots but a specific  
155 model was used for the 25-ha plot as this is known to have more slender trees  
156 (Vincent et al., 2014).

157 Above-ground biomass of each tree ( $AGB_t$ ) was estimated using the equa-  
158 tion in (Chave et al., 2005) :

$$AGB_t = 0.0509 \times \rho \times DBH^2 \times \bar{H} \quad (2)$$

159 where  $\bar{H}$  is the tree height estimated using the height-diameter equation  
160 1 and  $\rho$  is the oven-dry wood specific gravity in  $g/cm^3$ . A more recent allo-  
161 metric equation was published in (Chave et al., 2014) but it gave essentially  
162 identical AGB values (within 2%). Wood specific gravity  $\rho$ , was inferred from  
163 the species identification of the trees using a global wood density database  
164 (Chave et al., 2009). We assigned a  $\rho$  value to each tree corresponding to  
165 the mean  $\rho$  for species found in the database. Only  $\rho$  measurements made  
166 in tropical South America (4182 trees) were considered in order to limit the  
167 bias due to regional variation of wood density (Muller-Landau, 2004; Chave  
168 et al., 2006). When no reliable species identification or no wood density in-  
169 formation at the species level was available, the mean wood density at higher  
170 taxonomic level (i.e. genus, family) or at the plot level was attributed to the

171 tree. In each plot, AGB was summed across trees and normalized by plot  
172 area to obtain AGB density in t/ha, in dry biomass units (note that AGB in  
173 dry biomass units may be converted into carbon units using a 0.48 ratio).

### 174 *2.2. LiDAR data*

175 Airborne LiDAR campaigns were also conducted in the study sites to  
176 serve as a reference repository of canopy height estimates. In the Nouragues  
177 site, an airborne LiDAR survey was conducted in 2012, covering an area  
178 of 2400 ha. A canopy height model was generated from the cloud data at  
179 1-m resolution using the FUSION software ((McGaughey, 2012); Details on  
180 canopy model construction can be found in (Rejou-Mechain et al., 2015)  
181 ). At the Paracou study site, an airborne LiDAR survey was conducted in  
182 2008, covering an area of 1200 ha. The canopy model was generated by the  
183 ALTOA society using the TerraScan software ((Terrasolid, 2008); Details on  
184 the LiDAR data can be found in (Vincent et al., 2012)).

### 185 *2.3. SAR data-sets*

186 The TropiSAR study was conducted in the summer of 2009, and SAR  
187 airborne campaigns covered both Nouragues and Paracou sites flying mul-  
188 tiple baselines, so as to allow tomographic processing. The SAR system  
189 used in the TropiSAR campaign was the ONERA airborne system SETHI  
190 (Dubois-Fernandez et al., 2012). The P-band SAR had a bandwidth of 335  
191 - 460 MHz (125 MHz) and the resolution was 1 m in slant range and 1.245  
192 m in azimuth direction (Dubois-Fernandez et al., 2012). Datasets of the  
193 TropiSAR campaign are available as an ESA archive through the EOPI por-  
194 tal (<http://eopi.esa.int>).

195 At Nouragues, tomographic data-sets consisted of five fully polarimetric  
196 Single Look Complex (SLC) images at P-band acquired on 14 August 2009.  
197 The baselines have been spaced vertically with a spacing of 15 m. The flight  
198 trajectory was lower than the reference line (3962m) with a vertical shift of  
199 15 m, 30 m, 45 m and 60 m, respectively. At Paracou, tomographic data-  
200 sets consisted of 6 fully polarimetric SLC images at P-band (and L-band)  
201 acquired on 24 August 2009. As for Nouragues, the baselines had a spacing  
202 of 15 m with a reference line of 3962 m, but an additional vertical shift at 75  
203 m. In both data-sets, with the vertical shift of 15 m, the height of ambiguity  
204 was 110 m in near range and 210 m in far range, enabling unambiguous  
205 imaging of the forest volume.

206 Since the tomographic flight lines were in a vertical plane rather than in a  
207 horizontal plane, the phase to height factor and the height of ambiguity had a  
208 small variation across the scene swath (Dubois-Fernandez et al., 2012). The  
209 resulting vertical resolution is 20 m, whereas forest height ranges from 20 m  
210 to over 40 m. These features make it possible to map the 3-D distribution of  
211 the reflectivity by a coherent focusing, see section 2.4.

212 The Nouragues and Paracou SAR images are shown in Fig. 1. In the  
213 Nouragues image, almost the whole scene is forested except the Arataye river  
214 in the south and the top of the Inselberg in the northwest. In the Paracou  
215 image, the Sinnamary river and the bare terrain areas can be observed. In  
216 both images, the texture of the river and the bare terrain areas are uniform  
217 as compared to the forested areas.

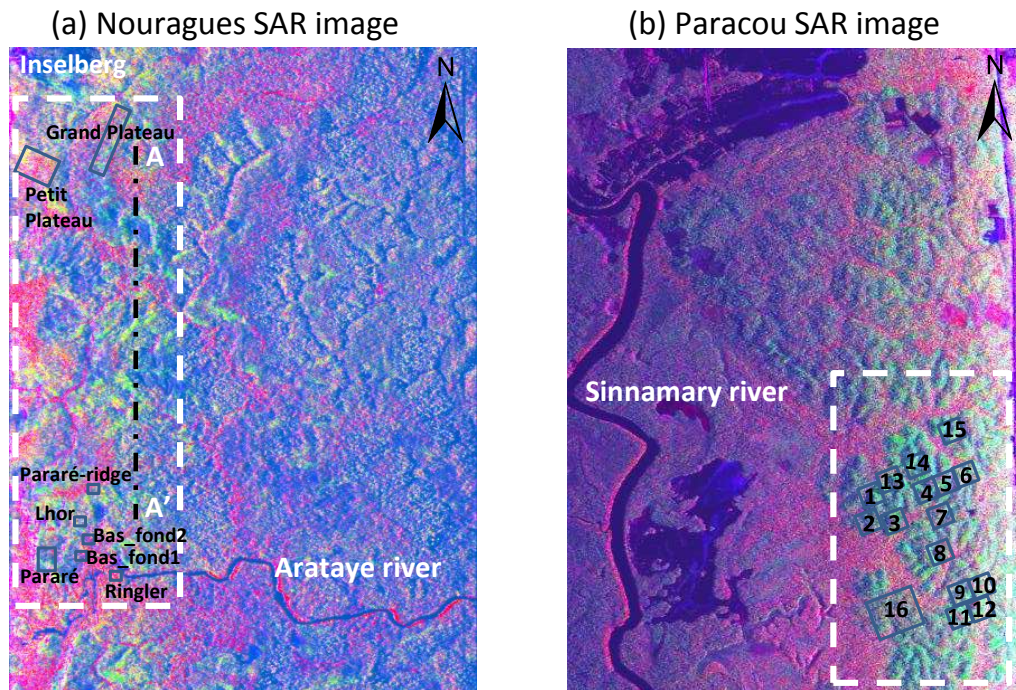


Figure 1: P-band SAR image (8 km x 6 km) in Pauli false color (R:  $|HH-VV|$ , G:  $2|HV|$ , B:  $|HH+VV|$ , where H and V refer to horizontal and vertical linear polarizations, respectively). The North is on the top. (a) Nouragues, the near range is on the left. (b) Paracou, the near range is on the right. The *in situ* AGB measurements are outlined with a label identifying the plot name. The white dash rectangles are relative to the area where LiDAR forest height data is available.

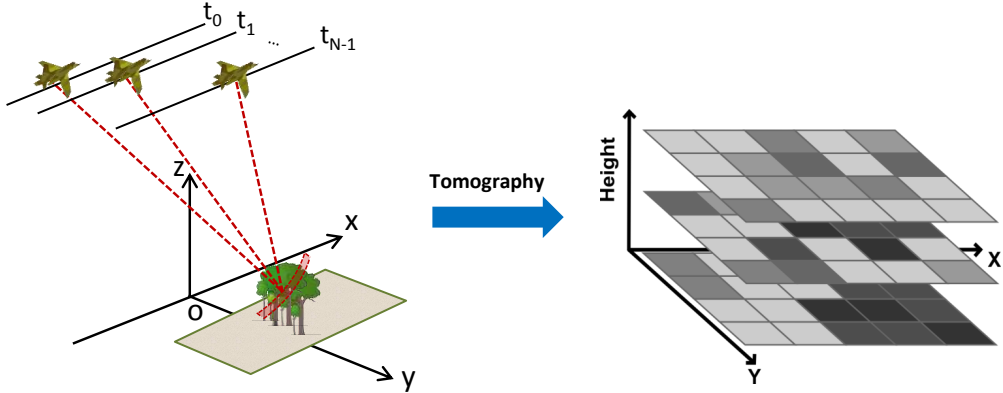


Figure 2: Left panel: a schematic view of the tomography acquisition. Right panel: multi-layer images, each of which represents scattering contributions associated with a certain height.

218 *2.4. TomoSAR processing*

219 The rationale of TomoSAR is to employ multiple flight tracks, nearly  
 220 parallel to each other, as shown in the left panel of figure 2. The ensemble  
 221 of all flight lines allows formation of a 2-D synthetic aperture, with the  
 222 possibility to focus the signal in the whole 3-D space. In other words, by  
 223 exploiting TomoSAR, multi-baseline SLC data can be converted into a new  
 224 multi-layer SLC data stack where each layer represents scattering contribu-  
 225 tions associated with a certain height, as shown in the right panel of figure  
 226 2.

227 Let us consider a multi-baseline data-set of SLC SAR images acquired  
 228 by flying the sensor along  $N$  parallel tracks, and let  $y_n(r, x)$  denote the pixel  
 229 at slant range, azimuth location  $(r, x)$  in the  $n$ -th image. Assuming that  
 230 each image within the data stack has been resampled on a common master

231 grid, and that phase terms due to platform motion and terrain topography  
 232 have been compensated, the following model holds (Bamler and Hartl, 1998;  
 233 Reigber and Moreira, 2000; Tebaldini, 2010):

$$y_n(r, x) = \int S(\xi, r, x) \exp\left(j \frac{4\pi}{\lambda r} b_n \xi\right) d\xi \quad (3)$$

234 where:  $b_n$  is the normal baseline relative to the  $n$ -th image with respect  
 235 to a common master image;  $\lambda$  is the carrier wavelength;  $\xi$  is the cross range  
 236 coordinate, defined by the direction orthogonal to the Radar Line-of-Sight  
 237 (LOS) and the azimuth coordinate;  $S(\xi, r, x)$  is the average scene complex  
 238 reflectivity within the slant range, azimuth, cross range resolution cell, as  
 239 shown in figure 3. Equation (3) states that SAR multi-baseline data and  
 240 the cross range distribution of the scene reflectivity constitute a Fourier pair.  
 241 Accordingly, the latter can be retrieved by taking the Fourier Transform of  
 242 the data along the baseline direction.

$$\hat{S}(\xi, r, x) = \sum_{n=1}^N y_n(r, x) \exp\left(-j \frac{4\pi}{\lambda r} b_n \xi\right) \quad (4)$$

243 As a result, TomoSAR processing allows us to retrieve the cross range  
 244 distribution of the scene complex reflectivity at each range and azimuth lo-  
 245 cation, hence providing fully 3-D imaging capabilities. The final conversion  
 246 from cross range to height is then obtained through straightforward geomet-  
 247 rical arguments. The resulting vertical resolution is approximately (Reigber  
 248 and Moreira, 2000):

$$\Delta z \simeq \frac{\lambda r \sin\theta}{2 b_{max}} \quad (5)$$

249 where  $\theta$  is the radar look angle and  $b_{max}$  the overall normal baseline span.  
 250 Equation (5) defines the so called Rayleigh limit. This way of processing does

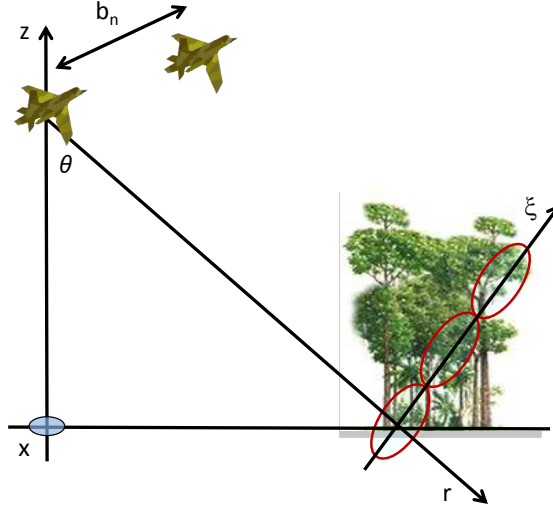


Figure 3: Schematic representation of the tomography geometry. Azimuth axis is orthogonal to the picture.

251 not optimize vertical resolution but ensures good radiometric accuracy in the  
 252 vertical direction. An alternative approach would be to resort to sophisti-  
 253 cated spectral estimation techniques such as MUSIC, CAPON, RELAX, or  
 254 Compressive sensing algorithms (Zhu and Bamler, 2010; Gini et al., Oct 2002;  
 255 Lombardini and Reigber, 2003). Such algorithms, however, are optimized for  
 256 the problem of detecting and localizing point targets, whereas they result in  
 257 poor radiometric accuracy in the case of distributed targets.

258 To apply the simple approach depicted above, it is usually necessary  
 259 to take a number of factors into account (Ho Tong Minh et al., 2014a).  
 260 First, the baseline distribution is not uniform due to atmospheric turbulences  
 261 affecting the airborne flight trajectory. Second, the phases of the SLC data  
 262 are affected by slow varying phase disturbances caused by uncompensated  
 263 platform motion. Both factors affect tomographic focusing, leading to a

264 blurring of the processed data, and hence need to be corrected. Third, terrain  
265 topography has to be considered, as it plays a key role for studying the  
266 relation between TomoSAR and in-situ measurements.

267 After these pre-processing steps, tomographic imaging is performed sim-  
268 ply by taking the Fourier Transform (with respect to the normal baseline)  
269 of the multi-baseline SLC data set at every slant range, azimuth location.  
270 The result of this operation is a multi-layer SLC stack, where each layer is  
271 referred to a fixed height above the terrain. We will hereinafter refer to each  
272 image within the multi-layer data stack simply by the associated height (i.e.:  
273 *15 m layer, 30 m layer...*), or as *ground layer* for the image focused at 0 m. A  
274 detailed step by step description of the processing is given in (Ho Tong Minh  
275 et al., 2014a). Fig. 4a and 4b show the HV backscatter for layers at ground  
276 layer 0 m, 15 m, and 30 m over the Nouragues and Paracou sites, respec-  
277 tively. To provide a comparison we also show the backscatter relative to one  
278 image from the original multi-baseline data-stack (i.e. non-tomographic).

279 We then evaluated the relationship between backscatter for different layer  
280 heights and in-situ AGB using the slope of a least-square linear regression  
281 and the Pearson coefficient  $r_P$ . It is well-known that the cross-polarization  
282 HV have a better correlation with AGB than the co-polarization HH or VV  
283 (see for instance (Ho Tong Minh et al., 2014a)). Hence to focus the discussion  
284 we only report on the HV results in this paper.

285 We define a simple AGB model assuming a classical log law:

$$AGB = a \times \log_{10}(P_L) + b, \quad (6)$$

286 where  $AGB$  is the estimated forest AGB,  $P_L$  is the HV backscatter of a



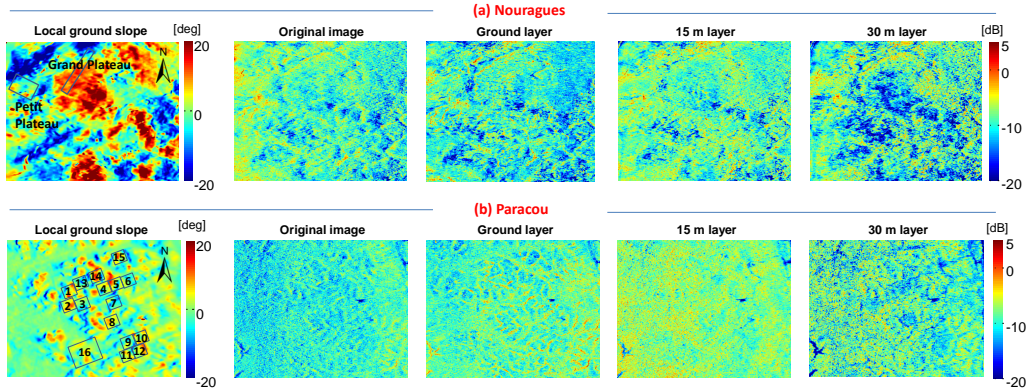


Figure 4: (a) Nouragues site, the left panel is the local ground slope and the right panels are HV intensities associated with the original (i.e. non-tomographic) SAR image with the three layer produced by TomoSAR. (b) Paracou site, the left panel is the local ground slope and the right panels are HV intensities associated with the original SAR image with the three layer produced by TomoSAR. Compared to Paracou site, the topography of the Nouragues site is very rugged.

287 given tomographic layer, and  $a, b$  are two parameters to be calibrated using  
 288 training data. These parameters were estimated by using 10 training samples  
 289 selected randomly out of 112 plots (i.e. calibration dataset). To assess model  
 290 performance, the retrieved AGB values were then compared with the in-situ  
 291 AGB of the remaining samples (i.e. validation dataset) to estimate the RMSE  
 292 of the model.

293 Finally, to simulate BIOMASS equivalent data we reprocessed the high-  
 294 resolution airborne data (125 MHz of bandwidth) to generate a new data  
 295 stack with 6 MHz bandwidth and an azimuth resolution of 12 m. The over-  
 296 all baseline span was fixed to the critical value of BIOMASS (4610 m), 6  
 297 passes were used, resulting in the height of ambiguity 110 m and the vertical  
 298 resolution 20 m (Ho Tong Minh et al., 2015b). Based on this reprocessed

299 data-set we examined the relationship of TomoSAR products to biomass.  
 300 The reader is referred to (Ho Tong Minh et al., 2015b) for the description  
 301 of the BIOMASS simulator, for which BIOMASS tomographic data were  
 302 emulated at the Paracou site.

### 303 2.5. Forest top height retrieval

304 In tropical rainforests, where canopy structure is more complex than any  
 305 other forest type, estimating forest top height in the field is a challenging  
 306 task because it is often hard to clearly identify the top leaf or branch of a  
 307 tree in the canopy. Due to its ability to accurately characterize the vertical  
 308 structure of tropical forests, TomoSAR can be used to estimate forest top  
 309 height. Forest vertical structure can be observed by taking a tomographic  
 310 profile, i.e. a slice of the multi-layer data stack (Fig. 5).

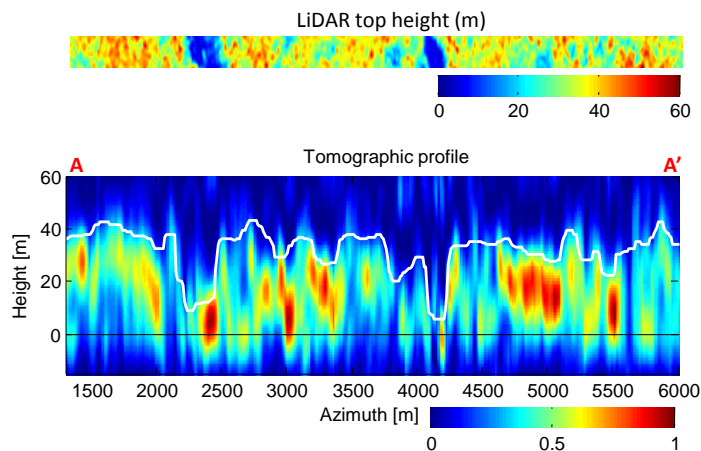


Figure 5: A tomographic profile at the Nouragures forest for the HV channel, see the black dashed line AA' in figure 1a. The power level for each channel is normalized in such a way that the level ranges from 0 (dark blue) to 1 (dark red). The top panels and the white line denote the LiDAR height measurements.

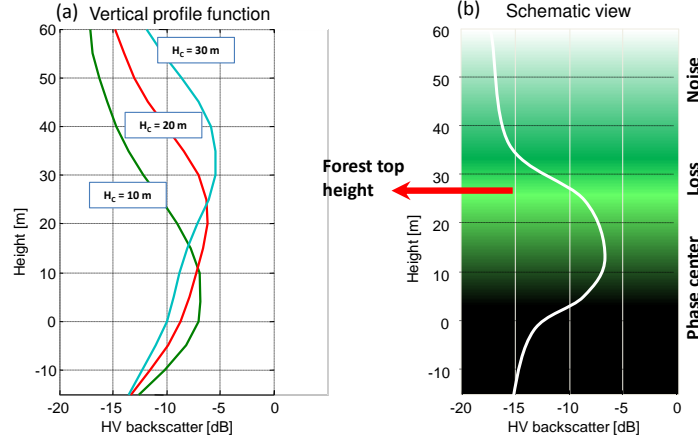


Figure 6: (a) The HV vertical backscatter distribution with respect to the phase center at 10 m, 20 m and 30 m, in Nouragues site. (b) The schematic view of the vertical backscatter distribution.

311 By retrieving the 3-D backscatter distribution from the multi-layer SLC,  
 312 it is possible to show the vertical backscatter distribution function. Each  
 313 vertical distribution is characterized by an effective scattering center, where  
 314 most of the backscatter is concentrated, the so called phase center  $H_C$ . This  
 315 can be written in formula,

$$H_C(r, x) = \arg \max \{P(z, r, x)\}, \quad (7)$$

316 where  $P(z, r, x)$  is the vertical backscatter at slant range, azimuth location  
 317  $(r, x)$  in vertical direction  $z$ . Figure 6a shows an example of HV vertical  
 318 backscatter distribution with respect to the phase center at 10 m, 20 m and  
 319 30 m, from the 3-D backscatter distribution in Nouragues site.

320 Fig. 6b shows a schematic view of the vertical backscatter distribution, in  
 321 which it can be assumed that the shape of the distribution can be divided into

322 three zones. The first corresponds to the zone where most of the backscatter  
 323 is concentrated, i.e. the phase center zone. The second is the power loss  
 324 zone, where the backscatter undergoes a loss along the vertical direction  
 325 from the phase center location. Further away, the backscatter is dominated  
 326 by noise, unlikely to be associated with any physically relevant components.  
 327 Therefore, by identifying the power loss from the phase center location in the  
 328 upper envelope of the profile, forest top height  $H$  can be retrieved (Tebaldini  
 329 and Rocca, 2012; Ho Tong Minh et al., 2015b). This can be written in  
 330 formula,

$$H(r, x) = \arg \min\{|P(z', r, x) - P(H_C, r, x) - K|\}, \quad (8)$$

331 where  $P(H_C, r, x)$  is the backscatter at phase center  $H_C$ ,  $K$  is the power  
 332 loss value,  $z'$  is the height values ranging from  $H_C$  to the upper envelope of  
 333 the profile, e.g. 60 m.

334 Since the forest top height retrieval is dependent on the choice of the  
 335 power loss value  $K$ , we used top-of-canopy height LiDAR models to select  
 336 an optimal power loss value.

### 337 **3. Results**

338 The three tomographic layers (0, 15 and 30 m) were found to be different  
 339 in their information content, with the upper vegetation layer (30 m) having  
 340 the highest correlation between the backscatter and AGB (Fig. 7). For this  
 341 layer, the Pearson correlation was 0.75 and the slope indicates an increase of  
 342  $> 1.8$  dB per 100 t/ha for a range of AGB of 200-600 t/ha. For the lower  
 343 layers, the linear correlations were weak, and even negative for the ground

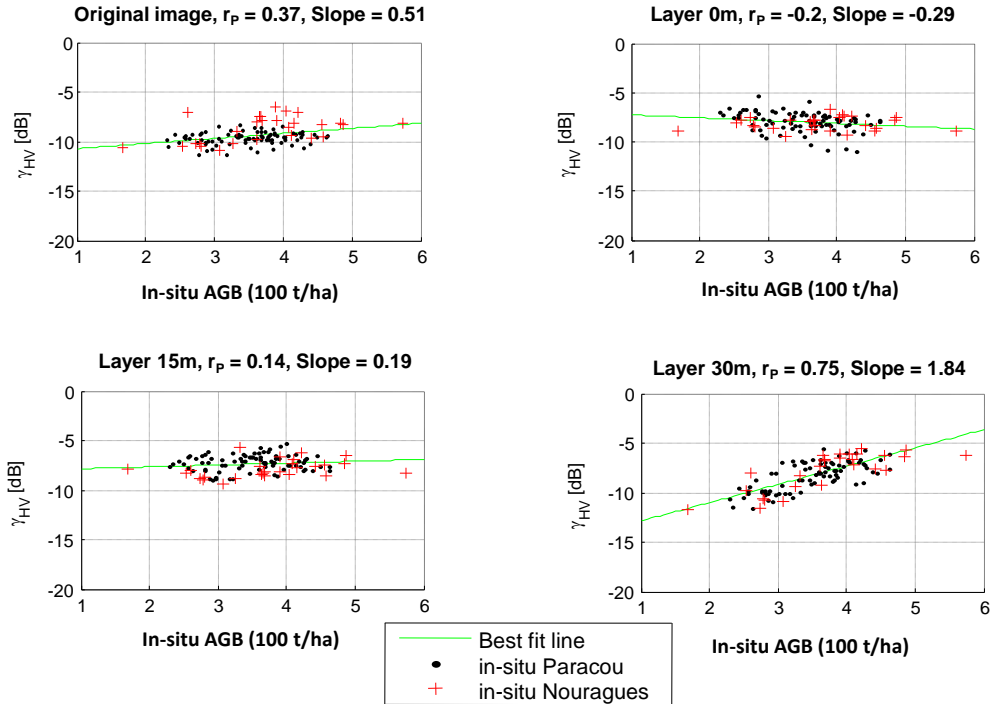


Figure 7: Sensitivity of HV backscatter at different layers produced by TomoSAR to above-ground biomass. The top left panel is the HV backscatter associated with the original SAR image.  $r_P$  is the Pearson correlation coefficient. Slope is referred to the angular coefficient of the resulting linear fit.

344 layer. Our results thus show that the best TomoSAR estimator to retrieve  
 345 AGB was based on the HV backscatter at 30 m. Results of the calibration  
 346 and validation with field data are reported in figure 8 and showed a model  
 347 RMSE of 15%.

348 Second, to test the robustness and transferability of the relationship be-  
 349 tween AGB and TomoSAR data, we used 27 plots from Nouragues for train-  
 350 ing and 85 samples from Paracou for validation, and vice versa. The RMSE  
 351 values from these cross-validation models were only slightly higher than to

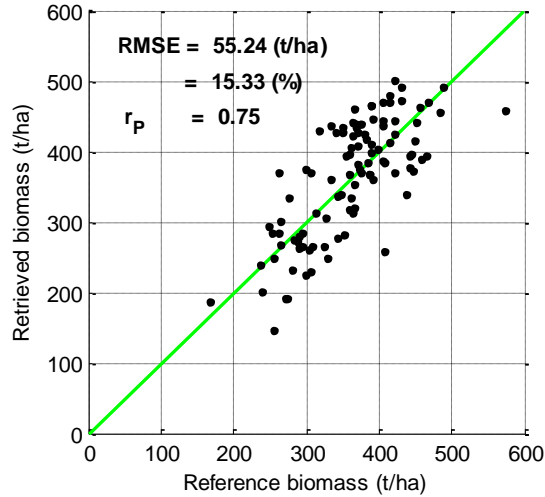


Figure 8: Comparison between in-situ AGB and AGB derived from inversion of the P-band HV 30 m layer, for both Paracou and Nouragues. The RMSE in retrieved AGB is 15.3% using 1-ha plots.

352 those obtained by using both training and validation samples from the same  
 353 study site (Fig. 9).

354 Third, we retrieved top heights from the tomographic profile (Fig. 5).  
 355 Using the top-of-canopy height LiDAR model we evaluated the forest top  
 356 height location corresponding to a power loss value, with respect to the phase  
 357 center, ranging from 0 to -10 dB (Fig. 10). In both the Nouragues and  
 358 Paracou sites, the bias associated with the TomoSAR top-height retrieval  
 359 decreased regularly with the power loss but the RMSE was significantly lower  
 360 at a power loss of 2 dB reaching only 2.5 m and 2 m in Nouragues and  
 361 Paracou, respectively. Using a power loss value of -2 dB at the Nouragues  
 362 and Paracou site, we then extrapolated the TomoSAR top-of-canopy height  
 363 retrieval estimates over the whole area covered by the LiDAR campaigns

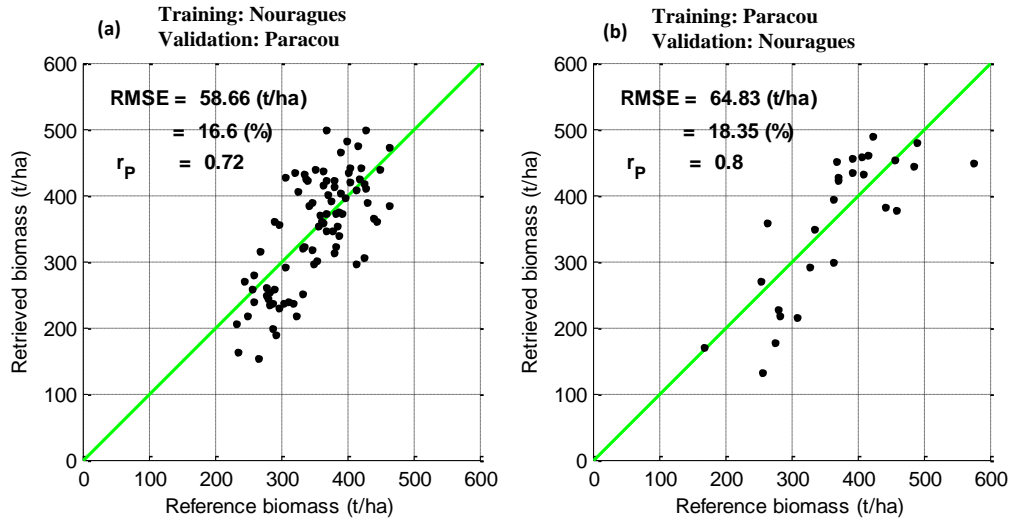


Figure 9: TomoSAR biomass retrieval result based on cross-validations: comparison of retrieved AGB and in-situ AGB. (a) training in Nouragues and validation in Paracou. (b) training in Paracou and validation in Nouragues

364 for comparison purpose (Fig. 11). Results show that the relative differences  
 365 between the top-of-canopy height LiDAR and TomoSAR estimates were 15%  
 366 for Nouragues and 10% for Paracou (Fig. 11 right panel).

367 In the Paracou forest the results from the emulated 6MHz-bandwidth sys-  
 368 tem were found to be similar with those obtained from the airborne dataset  
 369 in spite of the significant resolution loss. At the resolution of 4-ha, the RMSE  
 370 was 11% (Pearson correlation of 0.79). As shown in (Ho Tong Minh et al.,  
 371 2015b), it was possible to retrieve forest top height, in which the RMSE was  
 372 2.5 m, whereas the relative difference was 10%.

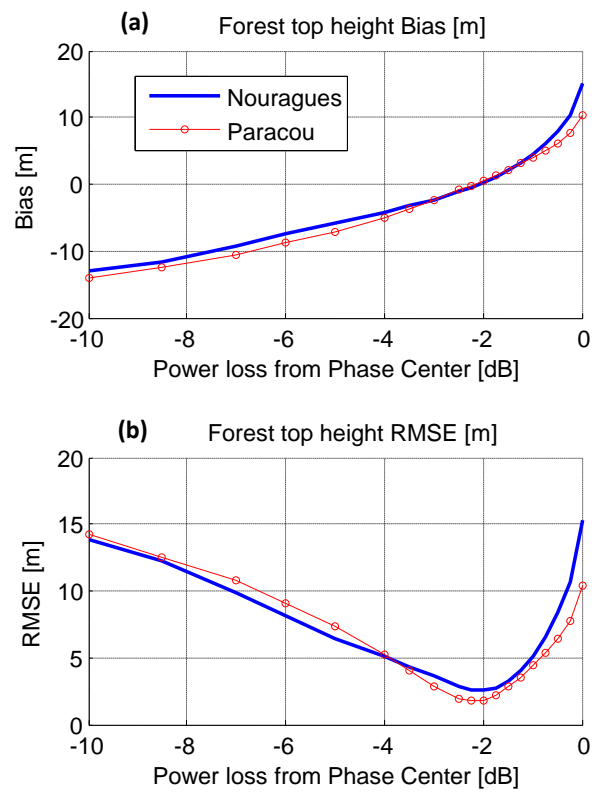


Figure 10: Forest top height bias and RMSE versus power loss with respect to phase center elevation. (a) Bias. (b) RMSE.



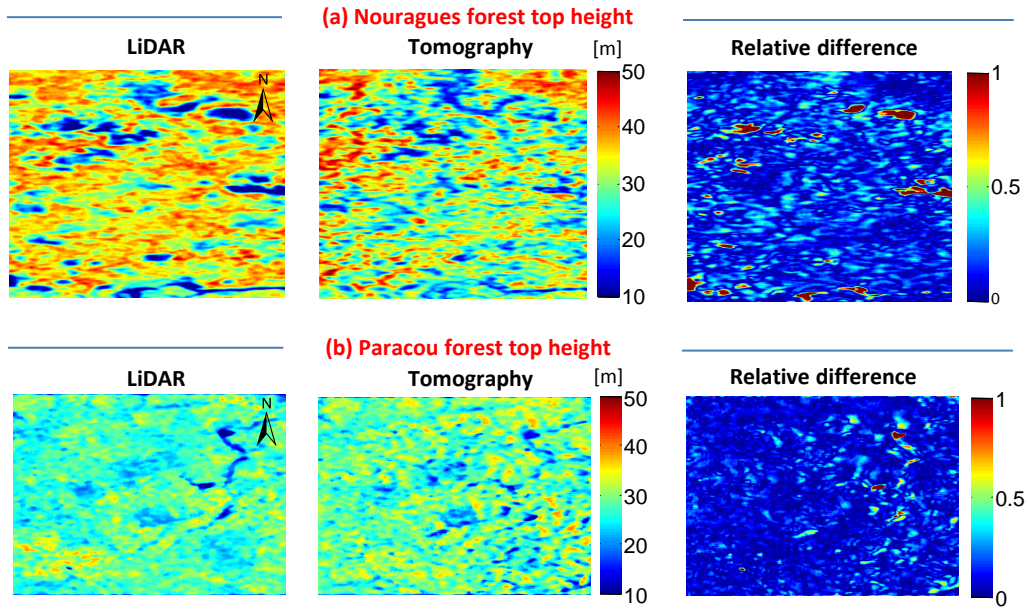


Figure 11: Comparison between LiDAR and tomography retrieval of forest top height in both sites. (a) Nouragues. (b) Paracou. The left panels show LiDAR height  $H_{LiDAR}$  available, see in Fig. 1. The middle panels present the results from tomography  $H_{tomography}$ . The right panels report the relative difference, defined by  $|H_{tomography} - H_{LiDAR}|/H_{LiDAR}$ .

#### 373 4. Discussion

374 In this work we show that TomoSAR approaches can be used to character-  
375 ize the vertical structure of tropical forests accurately, even over terrain with  
376 strong topography. The present analysis confirms the performance of the  
377 TomoSAR approach for aboveground biomass mapping in the tropics. AGB  
378 average relative errors were 15% at a 1-ha resolution, for both Nouragues and  
379 Paracou. Further, we demonstrate the stability of the TomoSAR retrieval  
380 method for different forest areas. Finally, we showed that canopy height re-  
381 trieval may be performed efficiently even in tropical forests on hilly terrain.  
382 Forest top height RMSE was estimated to be 2.5 m and 2 m for Nouragues  
383 and Paracou, respectively. Together these results considerably reinforce the  
384 proposal that BIOMASS, during its tomographic phase, will be able to pro-  
385 vide highly accurate wall-to-wall AGB mapping even in high carbon stock  
386 forests worldwide.

387 First, we showed that the same analysis conducted originally at a coastal  
388 tropical forest site of French Guiana, Paracou, could be replicated at an-  
389 other site (Nouragues), some 100 km away, and with independent ground  
390 data. This was expected to be challenging because the Nouragues area has a  
391 considerably more undulating terrain than Paracou, and this terrain is more  
392 typical of the Guiana Shield. Our study confirms that P-band SAR tomo-  
393 graphic data can retrieve AGB even on this terrain. This is reassuring given  
394 that many of the remaining mature tropical forests today are on steep slopes,  
395 inappropriate for cultivation (see table S4 in (Réjou-Méchain et al., 2014)).

396 In this paper, we also investigated whether our TomoSAR approach can  
397 be generalizable to other sites than the study site originally studied (Para-

398 cou), an important issue for the BIOMASS mission. The relationship be-  
399 tween AGB and TomoSAR data at Nouragues was found to be highly sim-  
400 ilar to the one observed in Paracou. In particular, we found that the best  
401 correlations hold in the upper layer (e.g., 30 m), whereas the ground and  
402 middle layers were poorly correlated to AGB. AGB retrieval using training  
403 plots from Nouragues and validation plots from Paracou, and vice versa, re-  
404 sulted in a RMSE of 16-18% using 1-ha plots, for AGB ranging from 200 to  
405 600 t/ha. This is a key result of this paper as it shows that the TomoSAR  
406 based biomass retrieval method is generalizable to other study sites at least  
407 to those forests with similar physiognomy, i.e. with canopy height ranging  
408 from 20 to 40 m. Hence, we provide support to the possibility to transfer  
409 training samples from one site to another, even if further studies should be  
410 conducted in other forests to assess the generality of our approach.

411 As previously discussed in (Ho Tong Minh et al., 2014a), the physical  
412 interpretation of these results is as follows. The correlation between the  
413 backscatter and AGB was very weak for the ground layer. Scatterers are  
414 indeed likely to be dispersed in the ground layer because dominant scatter-  
415 ing mechanisms are mostly influenced by local topographical or soil moisture  
416 variation. The relationship even tends to be negative, most probably because  
417 the signal extinction at the ground level is likely to be higher in the pres-  
418 ence of tall trees, and hence high AGB. In the 15-m layer, the correlation  
419 between backscatters and AGB was also weak. One possible explanation is  
420 that almost all trees from the stand may be represented in a rather similar  
421 way across sites in the 15-m layer. In recent studies, (Stegen et al., 2011)  
422 and (Slik et al., 2013) showed that only the largest trees ( $> 70$  cm of diame-

423 ter) drive the difference in AGB among sites and that smaller trees conveys  
424 no information on cross-sites differences in AGB. This may explain why the  
425 backscatter exhibited a strong significant correlation with AGB in upper lay-  
426 ers (20 m layer and higher), where the influence of large trees on backscatters  
427 prevails. Further, TomoSAR processing removes the ground contributions in  
428 the upper layers, minimizing the perturbing effects (e.g. local topography  
429 and/or soil moisture) associated with ground backscatter and thus improv-  
430 ing the relationship between AGB and backscatters.

431 We point out that the quality of our retrieval depended strongly on the  
432 availability of tomographic acquisitions. To place this result in perspective,  
433 we also used non-tomographic data (i.e. PolSAR) to infer AGB (Fig. 7).  
434 The non-tomographic data exhibit a much lower sensitivity to AGB ( $r_P =$   
435  $0.37$ ) than the tomographic data of the 30 m layer ( $r_P = 0.75$ , see top  
436 left panel of figure 7 ). The non-tomographic backscatter signals are more  
437 dispersed because they integrate noise signals from the ground, that need to  
438 be corrected with elaborate techniques (e.g. (Villard and Le Toan, 2015)),  
439 and signals from the middle layer that convey little information on AGB.

440 By evaluating the vertical forest structure from tomographic profiles, for-  
441 est top height can be retrieved. Using the LiDAR model as a reference, for  
442 Nouragues and Paracou, the same power loss value of -2 dB with respect to  
443 the phase center was used to retrieve forest height with no bias and mini-  
444 mum errors. The RMSE was estimated to be 2.5 m and 2 m, whereas the  
445 relative difference is 15% and 10%, for Nouragues and Paracou, respectively.  
446 This shows that the Nouragues hilly terrain is not a major limitation for the  
447 implementation of a canopy height retrieval algorithm with TomoSAR.

448 We note that the same power loss value can not be straightforwardly  
449 transferred to the case of other campaigns. As shown in (Tebaldini and  
450 Rocca, 2012) in the frame of the BioSAR 2008 campaign, the power loss  
451 should be varied in space due to a strong variation of the vertical resolution  
452 across the scene swath.

453 The results obtained above have to be carefully assessed in the context  
454 of a spaceborne satellite mission. In the case of the BIOMASS mission the  
455 limited pulse bandwidth of 6 MHz needs to be taken into account (ITU-  
456 2004, 2004). This low bandwidth has a significant effect on the resolution  
457 and quality of the TomoSAR products. At the proposed incidence angle of  
458  $23^{\circ}$ - $32^{\circ}$  of BIOMASS, the bandwidth reduction translates into a resolution  
459 loss not only in the horizontal direction but also in the vertical direction.  
460 Despite these effects, our simulation of BIOMASS-like data suggests that  
461 the performance loss of the TomoSAR derived products is not significant.  
462 Thus, our TomoSAR approach will be directly applicable to the BIOMASS  
463 mission.

464 In addition to resolution effects also other effects need to be taken into  
465 account when extrapolating the results of this study to the spaceborne case.  
466 These include ionosphere disturbances and temporal decorrelation effects.  
467 However, the impact of ionosphere, i.e. Faraday Rotation, was found not  
468 to be critical to TomoSAR (Tebaldini and Iannini, 2012). BIOMASS will  
469 acquire fully polarimetric data, therefore allowing estimation of Faraday Ro-  
470 tation to within an accuracy that will ensure a negligible impact on TomoSAR  
471 results. The impact of temporal decorrelation is under analysis in the frame  
472 of the TropiScat campaign activities (Ho Tong Minh et al., 2013, 2014b).

473 Temporal depends heavily on the repeat interval, which in the tomographic  
474 phase of the BIOMASS mission has been minimized to 3-4 days. The first  
475 attempt is provided in (Ho Tong Minh et al., 2015a), in which the resulting  
476 tomograms and forest heights were observed to change acceptably as long as  
477 the revisit time is 4 days or less.

478 To conclude, our results reinforce the science basis for the BIOMASS  
479 spaceborne mission. TomoSAR appears to be a promising technique to be  
480 used by BIOMASS for the retrieval of tropical forest biomass and height, and  
481 for the development of a training/validation strategy during the BIOMASS  
482 interferometric phase.

## 483 **5. Acknowledgements**

484 We thank the TropiSAR team for providing the TropiSAR datasets of  
485 excellent quality. We are grateful to the people and institutes that have  
486 contributed the field data, including L Blanc and B Hérault for Paracou,  
487 P Gaucher, P Châtelet, E Courtois, S Fauset, A Monteagudo, H. Richard  
488 and B Tymen for Nouragues, and G Vincent for tree height data in Paracou.  
489 Both Paracou and Nouragues are part of the Guyafor network. We gratefully  
490 acknowledge financial support from ESA (TropiSAR and TropiScat project),  
491 CNES (TOSCA program), from 'Investissement d'Avenir' grants managed  
492 by Agence Nationale de la Recherche (CEBA, ref. ANR-10-LABX-25-01;  
493 TULIP: ANR-10-LABX-0041; ANAEE-Services: ANR-11-INBS-0001) and  
494 from NERC ('AMAZONICA' consortium) and the Gordon and Betty Moore  
495 Foundation for contributing funding for field measurements at Nouragues  
496 through the RAINFOR project ([www.rainfor.org](http://www.rainfor.org)).

- 497 Baccini, A., Goetz, S. J., Walker, W. S., Laporte, N. T., Sun, M., Sulla-  
498 Menashe, D., Hackler, J., Beck, P. S. A., Dubayah, R., Friedl, M. A.,  
499 Samanta, S., Houghton, R. A., 2012. Estimated carbon dioxide emissions  
500 from tropical deforestation improved by carbon-density maps. *Nature Cli-*  
501 *mate Change* 2 (3), 182–185.
- 502 Bamler, R., Hartl, P., 1998. Synthetic aperture radar interferometry. *Inverse*  
503 *Problems* 14, R1–R54.
- 504 Blanc, L., Echard, M., Herault, B., Bonal, D., Marcon, E., Chave, J., Bar-  
505 aloto, C., 2009. Dynamics of aboveground carbon stocks in a selectively  
506 logged tropical forest. *Ecological Applications* 19 (6), 1397–1404.
- 507 Chave, J., Andalo, C., Brown, S., Cairns, M., Chambers, J., Eamus, D., Fol-  
508 ster, H., Fromard, F., Higuchi, N., Kir, T., Lescure, J.-P., Puig, H., Riera,  
509 B., Yamakura., T., Aug. 2005. Tree allometry and improved estimation of  
510 carbon stocks and balance in tropical forests. *Oecologia* 145, 87–99.
- 511 Chave, J., Coomes, D., Jansen, S., Lewis, S., Swenson, N., Zanne, A., 2009.  
512 Towards a worldwide wood economics spectrum. *Ecology Letters* 12, 351–  
513 366.
- 514 Chave, J., Muller-Landau, H., Baker, T., Easdale, T., Ter Steege, H., Webb,  
515 C., 2006. Regional and phylogenetic variation of wood density across 2456  
516 neotropical tree species. *Ecological Applications* 16, 2356–2367.
- 517 Chave, J., Rejou-Machain, M., Burquez, A., Chidumayo, E., Colgan, M. S.,  
518 Delitti, W. B., Duque, A., Eid, T., Fearnside, P. M., Goodman, R. C.,  
519 Henry, M., Martinez-Yrizar, A., Mugasha, W. A., Muller-Landau, H. C.,

- 520 Mencuccini, M., Nelson, B. W., Ngomanda, A., Nogueira, E. M., Ortiz-  
521 Malavassi, E., Pelissier, R., Ploton, P., Ryan, C. M., Saldarriaga, J. G.,  
522 Vieilledent, G., 2014. Improved allometric models to estimate the above-  
523 ground biomass of tropical trees. *Global Change Biology* 20 (10), 3177–  
524 3190.  
525 URL <http://dx.doi.org/10.1111/gcb.12629>
- 526 Dubois-Fernandez, P. C., Le Toan, T., Daniel, S., Oriot, H., Chave, J.,  
527 Blanc, L., Villard, L., Davidson, M. W. J., Petit, M., Aug. 2012. The  
528 TropiSAR airborne campaign in French Guiana: Objectives, description,  
529 and observed temporal behavior of the backscatter signal. *Geoscience and*  
530 *Remote Sensing, IEEE Transactions on* 8 (50), 3228–3241.
- 531 Gini, F., Lombardini, F., Montanari, M., Oct 2002. Layover solution in multi-  
532 baseline SAR interferometry. *Aerospace and Electronic Systems, IEEE*  
533 *Transactions on* 38 (4), 1344–1356.
- 534 Gourlet-Fleury, Guehl, S. J.-M., Laroussinie, O., 2004. Ecology and man-  
535 agement of a neotropical forest. Lessons drawn from Paracou, a long-term  
536 experimental research site in French Guiana. Elsevier, Paris.
- 537 Ho Tong Minh, D., Le Toan, T., Rocca, F., Tebaldini, S., Mariotti  
538 d’Alessandro, M., Villard, L., Feb 2014a. Relating P-band synthetic aper-  
539 ture radar tomography to tropical forest biomass. *Geoscience and Remote*  
540 *Sensing, IEEE Transactions on* 52 (2), 967–979.
- 541 Ho Tong Minh, D., Tebaldini, S., Rocca, F., Koleček, T., Borderies, P., Al-  
542 bilet, C., Villard, L., Hamadi, A., Le Toan, T., Aug 2013. Ground-based



543 array for tomographic imaging of the tropical forest in P-band. *Geoscience*  
544 *and Remote Sensing, IEEE Transactions on* 51 (8), 4460–4472.

545 Ho Tong Minh, D., Tebaldini, S., Rocca, F., Le Toan, T., June 2015a. The im-  
546 pact of temporal decorrelation on biomass tomography of tropical forests.  
547 *Geoscience and Remote Sensing Letters, IEEE* 12 (6), 1297–1301.

548 Ho Tong Minh, D., Tebaldini, S., Rocca, F., Le Toan, T., Borderies, P.,  
549 Koleček, T., Albinet, C., Hamadi, A., Villard, L., Aug 2014b. Vertical struc-  
550 ture of P-Band temporal decorrelation at the Paracou forest: Results from  
551 TropiScat. *Geoscience and Remote Sensing Letters, IEEE* 11 (8), 1438–  
552 1442.

553 Ho Tong Minh, D., Tebaldini, S., Rocca, F., Le Toan, T., Villard, L., Dubois-  
554 Fernandez, P., Feb 2015b. Capabilities of BIOMASS tomography for in-  
555 vestigating tropical forests. *Geoscience and Remote Sensing, IEEE Trans-*  
556 *actions on* 53 (2), 965–975.

557 ITU-2004, 2004. Article 5 (Frequency Allocations) of the radio regulations.  
558 International Telecommunication Union.

559 Le Toan, T., Beaudoin, A., Riom, J., Guyoni, D., Mar. 1992. Relating for-  
560 est biomass to SAR data. *IEEE Transactions on Geoscience and Remote*  
561 *Sensing* 30 (2), 403 – 411.

562 Le Toan, T., Quegan, S., Davidson, M., Balzter, H., Paillou, P., Papathanas-  
563 siou, K., Plummer, S., Rocca, F., Saatchi, S., Shugart, H., Ulander, L.,  
564 Jun. 2011. The BIOMASS Mission : Mapping global forest biomass to

- 565 better understand the terrestrial carbon cycle. *Remote Sensing of Envi-*  
566 *ronment*, 2850–2860.
- 567 Lombardini, F., Reigber, A., July 2003. Adaptive spectral estimation for  
568 multibaseline SAR tomography with airborne l-band data. In: *Geoscience*  
569 *and Remote Sensing Symposium, 2003. IGARSS '03. Proceedings. 2003*  
570 *IEEE International. Vol. 3. pp. 2014 – 2016.*
- 571 Mariotti d’Alessandro, M., Tebaldini, S., Rocca, F., 2013. Phenomenology  
572 of ground scattering in a tropical forest through polarimetric synthetic  
573 aperture radar tomography. *Geoscience and Remote Sensing, IEEE Trans-*  
574 *actions on* 51 (8), 4430–4437.
- 575 McGaughey, R., 2012. *Fusion/ldv: Software for lidar data analysis and visu-*  
576 *alization. US Department of Agriculture, Forest Service, Pacific Northwest*  
577 *Research Station: Seattle, WA, USA, 123.*
- 578 Mermoz, S., Rejou-Mechain, M., Villard, L., Toan, T. L., Rossi, V.,  
579 Gourlet-Fleury, S., 2015. Decrease of l-band {SAR} backscatter with  
580 biomass of dense forests. *Remote Sensing of Environment* 159 (0), 307 –  
581 317.  
582 URL <http://www.sciencedirect.com/science/article/pii/S0034425714005112>
- 583 Mitchard, E. T. A., Feldpausch, T. R., Brienen, R. J. W., Lopez-Gonzalez,  
584 G., Monteagudo, A., Baker, T. R., Lewis, S. L., Lloyd, J., Quesada, C. A.,  
585 Gloor, M., ter Steege, H., Meir, P., Alvarez, E., Araujo-Murakami, A.,  
586 Aragao, L. E. O. C., Arroyo, L., Aymard, G., Banki, O., Bonal, D., Brown,  
587 S., Brown, F. I., Ceron, C. E., Chama Moscoso, V., Chave, J., Comiskey,

588 J. A., Cornejo, F., Corrales Medina, M., Da Costa, L., Costa, F. R. C.,  
589 Di Fiore, A., Domingues, T. F., Erwin, T. L., Frederickson, T., Higuchi,  
590 N., Honorio Coronado, E. N., Killeen, T. J., Laurance, W. F., Levis, C.,  
591 Magnusson, W. E., Marimon, B. S., Marimon Junior, B. H., Mendoza Polo,  
592 I., Mishra, P., Nascimento, M. T., Neill, D., Nunez Vargas, M. P., Palacios,  
593 W. A., Parada, A., Pardo Molina, G., Pena-Claros, M., Pitman, N., Peres,  
594 C. A., Poorter, L., Prieto, A., Ramirez-Angulo, H., Restrepo Correa, Z.,  
595 Roopsind, A., Roucoux, K. H., Rudas, A., Salomao, R. P., Schiatti, J.,  
596 Silveira, M., de Souza, P. F., Steininger, M. K., Stropp, J., Terborgh, J.,  
597 Thomas, R., Toledo, M., Torres-Lezama, A., van Andel, T. R., van der  
598 Heijden, G. M. F., Vieira, I. C. G., Vieira, S., Vilanova-Torre, E., Vos,  
599 V. A., Wang, O., Zartman, C. E., Malhi, Y., Phillips, O. L., 2014. Markedly  
600 divergent estimates of amazon forest carbon density from ground plots and  
601 satellites. *Global Ecology and Biogeography* 23 (8), 935–946.

602 URL <http://dx.doi.org/10.1111/geb.12168>

603 Mitchard, E. T. A., Saatchi, S. S., Woodhouse, I. H., Nangendo, G., Ribeiro,  
604 N. S., Williams, M., Ryan, C. M., Lewis, S. L., Feldpausch, T. R., Meir,  
605 P., 2009. Using satellite radar backscatter to predict above-ground woody  
606 biomass: A consistent relationship across four different african landscapes.  
607 *Geophysical Research Letters* 36 (23), n/a–n/a, 123401.

608 URL <http://dx.doi.org/10.1029/2009GL040692>

609 Muller-Landau, H., 2004. Interspecific and inter-site variation in wood spe-  
610 cific gravity of tropical trees. *Biotropica* 36, 20–32.

611 Pan, Y., Birdsey, R. A., Fang, J., Houghton, R., Kauppi, P. E., Kurz, W. A.,

612 Phillips, O. L., Shvidenko, A., Lewis, S. L., Canadell, J. G., Ciais, P.,  
613 Jackson, R. B., Pacala, S. W., McGuire, A. D., Piao, S., Rautiainen, A.,  
614 Sitch, S., Hayes, D., 2011. A large and persistent carbon sink in the world's  
615 forests. *Science* 333, 988–993.

616 Reigber, A., Moreira, A., Sep. 2000. First demonstration of airborne SAR  
617 tomography using multibaseline L-band data. *IEEE Trans. on Geoscience*  
618 *and Remote Sensing*, 2142–2152.

619 Réjou-Méchain, M., Muller-Landau, H. C., Detto, M., Thomas, S. C.,  
620 Le Toan, T., Saatchi, S. S., Barreto-Silva, J. S., Bourg, N. A., Bunyave-  
621 jchewin, S., Butt, N., Brockelman, W. Y., Cao, M., Cárdenas, D., Chiang,  
622 J.-M., Chuyong, G. B., Clay, K., Condit, R., Dattaraja, H. S., Davies, S. J.,  
623 Duque, A., Esufali, S., Ewango, C., Fernando, R. H. S., Fletcher, C. D.,  
624 Gunatilleke, I. A. U. N., Hao, Z., Harms, K. E., Hart, T. B., Hérault,  
625 B., Howe, R. W., Hubbell, S. P., Johnson, D. J., Kenfack, D., Larson,  
626 A. J., Lin, L., Lin, Y., Lutz, J. A., Makana, J.-R., Malhi, Y., Marthews,  
627 T. R., McEwan, R. W., McMahon, S. M., McShea, W. J., Muscarella,  
628 R., Nathalang, A., Noor, N. S. M., Nytch, C. J., Oliveira, A. A., Phillips,  
629 R. P., Pongpattananurak, N., PUNCHI-Manage, R., Salim, R., Schurman, J.,  
630 Sukumar, R., Suresh, H. S., Suwanvecho, U., Thomas, D. W., Thompson,  
631 J., Uriarte, M., Valencia, R., Vicentini, A., Wolf, A. T., Yap, S., Yuan, Z.,  
632 Zartman, C. E., Zimmerman, J. K., Chave, J., 2014. Local spatial struc-  
633 ture of forest biomass and its consequences for remote sensing of carbon  
634 stocks. *Biogeosciences Discussions* 11 (4), 5711–5742.  
635 URL <http://www.biogeosciences-discuss.net/11/5711/2014/>

- 636 Rejou-Mechain, M., Tymen, B., Blanc, L., Fause, t. S., Feldpausch, T., Mon-  
637 teagudo, A., Phillips, O., Richard, H., Chave, J., 2015. Using repeated  
638 small-footprint LiDAR maps to infer spatial variation and dynamics of  
639 a high-biomass neotropical forest. *Remote Sensing of Environment* 169,  
640 93–101.
- 641 Saatchi, S. S., Harris, N. L., Brown, S., Lefsky, M., Mitchard, E. T. A.,  
642 Salas, W., Zutta, B. R., Buerman, W., Lewis, S. L., Hagen, S., Petrova,  
643 S., White, L., Silman, M., Morel, A., Jun 2011a. Benchmark map of forest  
644 carbon stocks in tropical regions across three continents. *Proceedings of*  
645 *the National Academy of Sciences of the United States of America* 108 (24),  
646 9899–9904.
- 647 Saatchi, S. S., Harris, N. L., Brown, S., Lefsky, M., Mitchard, E. T. A.,  
648 Salas, W., Zutta, B. R., Buermann, W., Lewis, S. L., Hagen, S., Petrova,  
649 S., White, L., Silman, M., Morel, A., 2011b. Benchmark map of forest  
650 carbon stocks in tropical regions across three continents. *Proceedings of*  
651 *the National Academy of Sciences* 108 (24), 9899–9904.  
652 URL <http://www.pnas.org/content/108/24/9899.abstract>
- 653 Sandberg, G., Ulander, L. M. H., Fransson, J. E. S., Holmgren, J., T. Le  
654 Toan, 2011. L- and P-band backscatter intensity for biomass retrieval in  
655 hemiboreal forest. *Remote Sensing of Environment* 115, 2874–2886.
- 656 Slik, J. W. F., Paoli, G., McGuire, K., Amaral, I., Barroso, J., Bastian,  
657 M., Blanc, L., Bongers, F., Boundja, P., Clark, C., Collins, M., Dauby, G.,  
658 Ding, Y., Doucet, J.-L., Eler, E., Ferreira, L., Forshed, O., Fredriksson, G.,  
659 Gillet, J.-F., Harris, D., Leal, M., Laumonier, Y., Malhi, Y., Mansor, A.,

- 660 Martin, E., Miyamoto, K., Araujo-Murakami, A., Nagamasu, H., Nilus, R.,  
661 Nurtjahya, E., Oliveira, A., Onrizal, O., Parada-Gutierrez, A., Permana,  
662 A., Poorter, L., Poulsen, J., Ramirez-Angulo, H., Reitsma, J., Rovero,  
663 F., Rozak, A., Sheil, D., Silva-Espejo, J., Silveira, M., Spironelo, W., ter  
664 Steege, H., Stevart, T., Navarro-Aguilar, G. E., Sunderland, T., Suzuki, E.,  
665 Tang, J., Theilade, I., van der Heijden, G., van Valkenburg, J., Van Do, T.,  
666 Vilanova, E., Vos, V., Wich, S., Woll, H., Yoneda, T., Zang, R., Zhang,  
667 M.-G., Zweifel, N., 2013. Large trees drive forest aboveground biomass  
668 variation in moist lowland forests across the tropics. *Global Ecology and*  
669 *Biogeography* 22 (12), 1261–1271.  
670 URL <http://dx.doi.org/10.1111/geb.12092>
- 671 Smith-Jonforsen, G., Ulander, L., Luo, X., Oct. 2005. Low vhf-band  
672 backscatter from coniferous forests on sloping terrain. *Geoscience and Re-*  
673  *mote Sensing, IEEE Transactions on* 43 (10), 2246–2260.
- 674 Stegen, J. C., Swenson, N. G., Enquist, B. J., White, E. P., Phillips, O. L.,  
675 JÅžrgensen, P. M., Weiser, M. D., Monteagudo Mendoza, A., Nunez Var-  
676 gas, P., 2011. Variation in above-ground forest biomass across broad cli-  
677 matic gradients. *Global Ecology and Biogeography* 20 (5), 744–754.  
678 URL <http://dx.doi.org/10.1111/j.1466-8238.2010.00645.x>
- 679 Tebaldini, S., may 2010. Single and multipolarimetric SAR tomography of  
680 forested areas: A parametric approach. *Geoscience and Remote Sensing,*  
681 *IEEE Transactions on* 48 (5), 2375 –2387.
- 682 Tebaldini, S., Iannini, L., april 2012. Assessing the performance of tomo-

683 graphic measurements from a P-band spaceborne SAR. Synthetic Aperture  
684 Radar, 2012. EUSAR. 9th European Conference on, 1–4.

685 Tebaldini, S., Rocca, F., Jan 2012. Multibaseline polarimetric SAR tomogra-  
686 phy of a boreal forest at P- and L-Bands. *Geoscience and Remote Sensing*,  
687 *IEEE Transactions on* 50 (1), 232–246.

688 ter Steege, H., Pitman, N. C. A., Phillips, O. L., Chave, J., Sabatier,  
689 D., Duque, A., Molino, J.-F., Prevost, M.-F., Spichiger, R., Castellanos,  
690 H., von Hildebrand, P., Vasquez, R., 2006. Continental-scale patterns of  
691 canopy tree composition and function across amazonia. *Nature* 443, 444–  
692 447.

693 Terrasolid, 2008. Terrasolid : Software for processing lidar point clouds and  
694 images. Software for Processing LiDAR.

695 Van Zyl, J., Jan. 1993. The effect of topography on radar scattering from  
696 vegetated areas. *IEEE Transactions on Geoscience and Remote Sensing*  
697 31 (2), 153–160.

698 Villard, L., Le Toan, T., Jan 2015. Relating p-band sar intensity to biomass  
699 for tropical dense forests in hilly terrain:  $\gamma_0$  or  $t_0$ . *Selected Topics in*  
700 *Applied Earth Observations and Remote Sensing*, *IEEE Journal of* 8 (1),  
701 214–223.

702 Vincent, G., Sabatier, D., Blanc, L., Chave, J., Weissenbacher, E., Pelissier,  
703 R., Coutron, P., 2012. Accuracy of small footprint airborne LiDAR in  
704 its predictions of tropical moist forest stand structure. *Remote sensing of*  
705 *environment* 125, 23–33.

- 706 Vincent, G., Sabatier, D., Rutishauser, E., 2014. Revisiting a universal air-  
707 borne lidar approach for tropical forest carbon mapping: scaling-up from  
708 tree to stand to landscape. *Oecologia* 2 (175), 439–443.
- 709 Wright, S. J., Oct. 2005. Tropical forests in a changing environment.  
710 *TRENDS in Ecology and Evolution* 20 (10), 553–560.
- 711 Zhu, X. X., Bamler, R., dec. 2010. Very high resolution spaceborne SAR  
712 tomography in urban environment. *Geoscience and Remote Sensing, IEEE*  
713 *Transactions on* 48 (12), 4296 –4308.